A nonorthogonal CI treatment of symmetry breaking in sigma formyloxyl radical

Philippe Y. Ayala and H. Bernhard Schlegel

Citation: The Journal of Chemical Physics **108**, 7560 (1998); doi: 10.1063/1.476190
View online: http://dx.doi.org/10.1063/1.476190
View Table of Contents: http://scitation.aip.org/content/aip/journal/jcp/108/18?ver=pdfcov
Published by the AIP Publishing

A nonorthogonal CI treatment of symmetry breaking in sigma formyloxyl radical

Philippe Y. Ayala and H. Bernhard Schlegel
Department of Chemistry, Wayne State University, Detroit, Michigan 48202

(Received 8 August 1997; accepted 2 February 1998)

Spatial symmetry breaking can occur in Hartree–Fock wave functions when there are two or more close lying configurations that can mix strongly, such as in HCO_2, NO_2, and allyl radical. Like spin contamination, spatial symmetry breaking can cause sizeable errors when perturbation theory is used to estimate the correlation energy. With conventional methodology, very large MCSCF and MRCI calculations are necessary to overcome the spatial symmetry breaking problem. This paper explores an alternative approach in which a 2×2 nonorthogonal CI is used to recombine the two symmetry broken Hartree–Fock determinants. The necessary matrix elements closely resemble those used in the spin projection calculations. Second order perturbation theory is used to include electron correlation energy in this approach. With perturbative corrections for correlation energy, this approach predicts that the $^2B_2$ structure is a minimum, in agreement with the best available calculations. © *1998 American Institute of Physics.* [S0021-9606(98)00218-9]

INTRODUCTION

The formyloxyl radical, HCO_2, is of particular interest in atmospheric and combustion chemistry as an intermediate in the $OH+CO \rightarrow H+CO_2$ reaction.[1–5] The formyloxyl radical is also a possible intermediate in the thermal decomposition of formic acid.[6–8] Despite its importance, relatively little is known experimentally about HCO_2, not even its equilibrium structure. Formyloxyl radical is also a very difficult system to study by quantum mechanical methods. Most correlated methods based on single determinants incorrectly predict that the equilibrium geometry has nonequivalent C–O bonds.[2,8] Similar to the isoelectronic allyl radical,[9,10] C_3H_5, and nitrogen dioxide,[11–16] NO_2, the Hartree–Fock wave function of the formyloxyl radical[16–22] suffers from spatial symmetry breaking (also known as artifactual symmetry breaking[11] or doublet instability[23,24]). However, a C_{2v} equilibrium geometry for HCO_2 can be obtained with extensive and carefully constructed multiconfiguration self-consistent field (MCSCF) and multireference configuration interaction (MRCI) calculations[16–20] or large EOM-CC calculations using the anion as a reference configuration.[21,22] In this paper we use the broken symmetry Hartree–Fock orbitals to construct a compact, high symmetry wave functions for the $^2B_2$ and $^2A_1$ states of the σ radicals of HCO_2, employing a 2×2 nonorthogonal configuration interaction[10,13,26,27] combined with second order perturbation theory (Scheme 1).

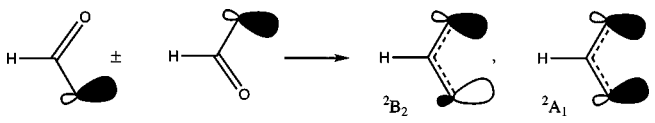

Scheme 1. Localized, broken symmetry configurations combined to form the $^2B_2$ and $^2A_1$ states of σ-HCO_2

The breaking of spatial symmetry in SCF wave functions has been examined a number of times during the last few decades by numerous groups.[9–46] This problem is often studied in the context of polyenes, open shell oxygen containing radicals, excited states and ions. Molecular systems that encounter symmetry-breaking problems in their wave function share a number of features. For a symmetry adapted HF wave function, minute antisymmetric displacements can cause discontinuous changes in the energy. Removal of the symmetry constraints on the HF wave function yields two or more lower energy wave functions and results in extensive relaxation of the molecular orbitals. The potential energy surfaces for these are continuous under distortions to lower symmetry and distortion to lower symmetry is energetically favored. Symmetry breaking in an HF wave function can occur if there are two or more single determinantal wave functions that (a) are similar in energy but different in symmetry, (b) differ by a single excitation and (c) can interact when the geometry is distorted to lower symmetry.[12,13]

McLean *et al.*[17] have used He_2^+ to clearly illustrate the problem of symmetry breaking in the SCF solution and especially the effect of orbital relaxation. A symmetry broken Hartree–Fock wave function, $\Psi_0=|\phi_a^2\phi_b'|$, is shown in Scheme 2; because the orbital localized on atom a has to accommodate two electrons, ϕ_a is significantly larger (more diffuse) than ϕ_b', the one localized on atom b. The configuration $|\phi_a\phi_b'^2|$ is considerably higher in energy because two electrons are placed in a smaller, more compact orbital. In the other symmetry broken wave function $P\Psi_0=|\phi_a'\phi_b^2|$, where P is the appropriate symmetry operator), ϕ_b^2 is larger than ϕ_a'.

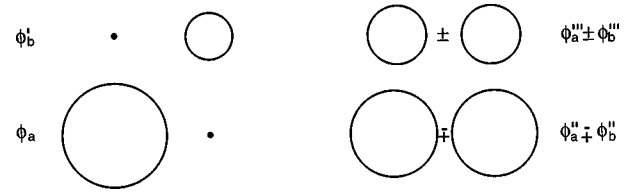

Scheme 2. Symmetry broken and symmetry constrained orbitals for He_2^+.

Alternatively one can construct two symmetry adapted Hartree–Fock wave functions (*gerade* and *ungerade*) from the localized orbitals on atoms a and b: $\Psi_{g,u} = |(\phi_a'' m \phi_b'')^2(\phi_a''' \pm \phi_b''')| = |\phi_b''^2 \phi_a'''| \pm |\phi_a''^2 \phi_b'''| + |\phi_a''^2 \phi_a'''| \pm |\phi_b''^2 \phi_b'''| +$ other contributions. By expanding the determinant, it can be clearly seen that the symmetry adapted wave functions contain configurations that resemble Ψ_0 and $P\Psi_0$. These terms, namely, $|\phi_b''^2 \phi_a'''|$ and $|\phi_a''^2 \phi_b'''|$, interact in a resonance fashion. However, $\Psi_{g,u}$ also contain $|\phi_a''^2 \phi_a'''|$ and $|\phi_b''^2 \phi_b'''|$ which correspond to high energy, ionic configurations. These terms are inherent to the symmetry constraints and the SCF process must find optimal orbital sizes that are a compromise between maximizing the resonance effect and minimizing the destabilization effect of the high energy ionic configurations. In the symmetry broken wave functions, such a compromise on orbital size is not necessary. The ordering of the orbital size is $\phi > \phi'' > \phi''' > \phi'$. This change in orbital size along with the localization constitutes the substantial orbital relaxation that accompanies symmetry breaking. From this, it can be inferred that the artifactual symmetry breaking problem appears when the two contradictory objectives of resonance and optimal orbital size cannot be achieved in a single determinant wave function. At shorter internuclear distances the resonance effect dominates and the symmetry adapted wave function is lower in energy; at larger distances the resonance effect is diminished and the broken symmetry wave function with its optimal size orbitals is more stable. Since single reference methods have problems balancing these two objectives, multiconfiguration SCF methods are usually used.

The MCSCF studies of the HCO_2 potential energy surface by Feller *et al.*,[19] McLean *et al.*,[17] and Rauk *et al.*[18] are among the most extensive. Feller, Davidson, and co-workers[19] used a split valence plus polarization basis set and 11 orbital/13 electron MCSCF restricted to no more than double excitations, followed by MRCI calculations. McLean *et al.*[17] carefully constructed a larger active space for σ-HCO_2 that included the CO, CO′, and CH σ and σ^* orbitals, the 3π orbitals and two in-plane p orbitals of different size on each oxygen to handle the orbital relaxation effect of the σ lone pairs and included dynamic correlation by MRCI calculations constrained to single and double excitations of the 12 most important reference functions. Rauk *et al.*[18] used complete active space MCSCF calculations with 11 electron in 13 orbitals, followed by multireference second order perturbation theory (CASPT2).[47] More recently, Stanton *et al.*[21,22] applied the EOM-CC method to HCO_2, using the anion as a reference determinant. This is effectively a multireference coupled cluster approach starting from all singly ionized determinants that can be generated from HCO_2^-. Small MCSCF and MRCI calculations find the $^2B_2$ structure to be a saddle point with respect to asymmetric C–O stretching; however, in larger MCSCF calculations, or with MRCI, CASPT2, or EOM-CC methods, the $^2B_2$ state is a minimum with an asymmetric C–O stretching frequency near 1000 cm^{-1} and, except for the CASPT2 calculations, is lower in energy than the $^2A_1$ structure.[16–22] The surface around the $^2A_1$ structure is very flat, and different levels of theory yield different results. With small to medium size basis sets, $^2A_1$ structure is a saddle point with respect to asymmetric C–O stretching,[16–22] but it may be a minimum with very large basis sets.[22] The $^2A_1$ structure can also dissociate to $H+CO_2$, with or without a small barrier, depending on the computational approach.[18,19] The $^2B_2$ and $^2A_1$ regions of the surface are connected via a pair C_s symmetry reaction paths with unequal C–O bond lengths; there may be minima and/or a small barrier along this path, depending on the level of theory.[16–22]

There are a number of additional studies on other systems that are related to the present work. Bartlett and co-workers[15,35–37] have studied spatial symmetry breaking in NO_2 and NO_3 using the Brueckner doubles method and coupled cluster wave functions with quasirestricted open shell orbitals. Hiberty *et al.*[48] have used a two configuration valence bond method with breathing orbitals to handle the orbital size effect in two center, three electron bonds. Burton *et al.*[16] have examined the vibrational frequencies in NO_2 and HCO_2 and have pointed out that the anomalously high frequencies for the asymmetric stretch found for symmetry constrained HF calculations are due to wavefunction instability with respect to symmetry breaking.

NONORTHOGONAL CI APPROACH

It would be very desirable to treat the symmetry breaking problem without having to resort to large MCSCF and MRCI calculations. In the two symmetry broken Hartree–Fock solutions for HCO_2, the orbitals are optimal size, whereas in the symmetry constrained $^2A_1$ and $^2B_2$ solutions, the resonance effect competes with the energy raising effect of intermediate size orbitals. One way to cope with this is to combine the two symmetry broken solutions with a simple 2×2 nonorthogonal configuration interaction scheme.[10,13,26,27] Jackels and Davidson[13] found that a 2×2 nonorthogonal CI was not adequate to reproduce a C_{2v} minimum for the $^2B_2$ state of NO_2, which is isoelectronic with HCO_2. Blahous *et al.*[14] suggest that this is due to the nearby crossing between the $^2A_1$ and $^2B_2$ surfaces; extensive CASSCF calculations show that additional configurations mix strongly, resulting in a C_{2v} minimum for the $^2B_2$ surface (but with a barrier of less than 1.8 kcal/mol for crossing to the $^2A_1$ surface). The HCO_2 surface may show similar difficulties, with added complications arising from transition states for C–H bond dissociation and 1, 2 hydrogen shifts.

A 2×2 nonorthogonal configuration interaction approach involves two sets of nonorthogonal orbitals and is similar to spin-coupled valence bond theory[49] and resonating GVB theory.[10,26] Let Ψ_0 and Ψ_0' be the two symmetry broken, normalized Hartree–Fock solutions; a symmetry adapted wave function Φ_0 can be constructed from a linear combination of Ψ_0 and Ψ_0' by solving a 2×2 nonorthogonal CI problem

$$\begin{bmatrix} E_0 & H \\ H & E_0' \end{bmatrix}\begin{bmatrix} d_0 \\ d_0' \end{bmatrix} = E\begin{bmatrix} 1 & S \\ S & 1 \end{bmatrix}\begin{bmatrix} d_0 \\ d_0' \end{bmatrix},$$
$$\Phi_0 = d_0\Psi_0 + d_0'\Psi_0', \tag{1}$$
$$E_0 = \langle\Psi_0|\mathbf{H}|\Psi_0\rangle, \quad E_0' = \langle\Psi_0'|\mathbf{H}|\Psi_0'\rangle,$$
$$H = \langle\Psi_0|\mathbf{H}|\Psi_0'\rangle, \quad S = \langle\Psi_0|\Psi_0'\rangle.$$

The matrix elements can be obtained by expanding one of the wave functions in terms of ground state and excited determinants of the obtained from the other wave function

$$\Psi_0' = a_0\Psi_0 + \sum a_i^a\Psi_i^a + \sum a_{ij}^{ab}\Psi_{ij}^{ab} + \cdots, \tag{2}$$

$$\langle\Psi_0|\mathbf{H}|\Psi_0'\rangle = a_0\langle\Psi_0|\mathbf{H}|\Psi_0\rangle + \sum a_{ij}^{ab}\langle\Psi_0|\mathbf{H}|\Psi_{ij}^{ab}\rangle. \tag{3}$$

The coefficients a_i^a, a_{ij}^{ab} etc. can be obtained from the overlaps between the two sets of orbitals, as outlined in the Appendix.

For symmetric geometries, Ψ_0 and Ψ_0' are energetically equivalent and molecular orbitals of Ψ_0' can be obtained by applying the appropriate symmetry operator to the molecular orbitals of Ψ_0. For lower symmetry geometries, the orbitals are obtained from two separate SCF calculations; however, converging two separate UHF localized solutions can be difficult. A semiempirical initial guess for the wave function does not necessarily converge to the lowest energy broken symmetry state, but a suitable initial guess for the second state can be obtained by permuting the orbital coefficients from the converged solution of the first state. Both solutions are stable with respect to quadratic displacements of the MO coefficients (i.e., the orbital rotation hessians have only positive eigenvalues).

Perturbation theory can be used to estimate the electron correlation contributions to the wave functions associated with each symmetry broken solution. Let the wave function for the system be a linear combination of the two perturbationally corrected symmetry broken solutions

$$\Psi = \Psi_0 + \Psi_1 + \Psi_2 + \cdots; \quad \Psi' = \Psi_0' + \Psi_1' + \Psi_2' + \cdots,$$
$$\Phi = d\Psi + d'\Psi'. \tag{4}$$

The coefficients and correlated energy can be obtained by solving a suitable 2×2 eigenvalue problem, in which the matrix elements are evaluated in the spirit of perturbation theory, i.e., retaining terms up to a given order (in some respects, this is akin to quasidegenerate perturbation theory). The diagonal elements are the respective perturbational energies of the symmetry broken solutions and pose no problems. The off-diagonal matrix elements are taken as the average of the two possible forms so that the matrices are hermitian in the low symmetry cases. For second order the equations are

$$\begin{bmatrix} E_{\mathrm{MP2}} & H \\ H & E_{\mathrm{MP2}}' \end{bmatrix}\begin{bmatrix} d \\ d' \end{bmatrix} = E\begin{bmatrix} 1 & S \\ S & 1 \end{bmatrix}\begin{bmatrix} d \\ d' \end{bmatrix},$$
$$\Phi = d_0(\Psi_0 + \Psi_1) + d_0'(\Psi_0' + \Psi_1'),$$
$$E_{\mathrm{MP2}} = \langle\Psi_0|\mathbf{H}|\Psi_0 + \Psi_1\rangle, \quad E_{\mathrm{MP2}}' = \langle\Psi_0'|\mathbf{H}|\Psi_0' + \Psi_1'\rangle, \tag{5}$$
$$H = (\langle\Psi_0|\mathbf{H}|\Psi_0' + \Psi_1'\rangle + \langle\Psi_0'|\mathbf{H}|\Psi_0 + \Psi_1\rangle)/2,$$
$$S = (\langle\Psi_0|\Psi_0' + \Psi_1'\rangle + \langle\Psi_0'|\Psi_0 + \Psi_1\rangle)/2.$$

The off-diagonal Hamiltonian matrix element $\langle\Psi_0'|\mathbf{H}|\Psi_1\rangle$ requires Ψ_0' in Eq. (2) to be expanded up to fourth order. The resulting expression resembles the CCSD equations, and can be evaluated with very little modification of the CCSD code. The computational work is comparable to one CCSD iteration or an MP4SDQ calculation.

The correlation corrections to the 2×2 nonorthogonal CI equations can also be approximated in a manner similar to spin projected Møller–Plesset perturbation theory. In this approach, the energy expression is very similar to the approximate spin projected MP2 energy used in a number of previous studies by Schlegel.[50] Equation (2) can be rewritten as

$$\Psi_0' = \langle\Psi_0|\Psi_0'\rangle\Psi_0 + \tilde{\Psi}, \tag{6}$$

where $\tilde{\Psi}$ is linear combination of excited determinants built from Ψ_0. An approximate expression for Ψ' can be obtained by assuming the perturbative corrections to $\tilde{\Psi}$ are small

$$\Psi' = \Psi_0' + \Psi_1' \cdots$$
$$\approx \langle\Psi_0|\Psi_0'\rangle(\Psi_0 + \Psi_1\cdots)$$
$$+ \tilde{\Psi}(1 - \langle\tilde{\Psi}|\Psi_1\cdots\rangle/\langle\tilde{\Psi}|\tilde{\Psi}\rangle). \tag{7}$$

The last term is included to remove from $\tilde{\Psi}$ any contributions already contained in Ψ_1. The approximate off-diagonal hessian can then be computed relatively simply

$$\langle\Psi_0|\mathbf{H}|\Psi'\rangle \approx \langle\Psi_0|\Psi_0'\rangle\langle\Psi_0|\mathbf{H}|\Psi_0 + \Psi_1\cdots\rangle$$
$$+ \langle\Psi_0|\mathbf{H}|\tilde{\Psi}\rangle(1 - \langle\tilde{\Psi}|\Psi_1\cdots\rangle/\langle\tilde{\Psi}|\tilde{\Psi}\rangle). \tag{8}$$

For the high symmetry case when $\langle\Psi_0|\mathbf{H}|\Psi_0\rangle = \langle\Psi_0'|\mathbf{H}|\Psi_0'\rangle$, the energy for the 2×2 CI reduces to

$$E \approx E_{\mathrm{MP2}} + \Delta E_0(1 - \langle\tilde{\Psi}|\Psi_1'\rangle/\langle\tilde{\Psi}|\tilde{\Psi}\rangle), \tag{9}$$

where $\Delta E_0 = \langle\Psi_0|\mathbf{H}|\tilde{\Psi}\rangle/(1 + \langle\Psi_0|\Psi_0'\rangle)$ is the energy lowering given by the 2×2 CI based on Hartree–Fock determinants, Eq. (1). This scheme has a significantly lower computational cost than Eq. (5). These two schemes can be shown to yield a continuous PES, even as the symmetry broken UHF solutions disappear. The energy gradient is continuous except at the onset of the symmetry breaking instability.

Calculations were carried out with the GAUSSIAN series of programs[51] using the spin unrestricted Hartree–Fock (UHF) method with a split valence plus polarization basis set (6-31G*). Additional code was written to compute the matrix elements needed for the nonorthogonal CI and the MP2 corrections based on the symmetry broken determinants. Vibrational frequencies were calculated by double numerical differentiation. Because the σ and π states are very close in energy, converging to the desired σ UHF solutions required some care.

TABLE I. Energies and optimized geometries of $^2B_2$ σ-HCO_2 calculated with single reference, symmetry constrained wave functions and the 6-31G* basis set.

Method	CH (Å)	CO (Å)	HCO (degree)	OCO (degree)	Energy (Hartree)	ΔE^b (kcal/mol)
HF	1.0859	1.2311	123.87	112.26	−188.094 168	−9.78
B3LYP	1.1000	1.2564	123.44	113.11	−189.078 964	0.00
MP2	1.0945	1.2598	124.25	111.50	−188.578 110	10.81
QCISD	1.0986	1.2615	123.78	112.44	−188.592 387	−2.86
QCISD(T)[a]	1.0995	1.2678	123.70	112.60	−188.600 209	14.00
CCSD	1.0978	1.2576	123.82	112.36	−188.587 621	0.93
CCSD(T)	1.0996	1.2647	123.70	112.60	−188.607 549	1.57
BD[a]	1.0983	1.2564	123.87	112.26	−188.574 838	0.02
BD(T)[a]	1.0996	1.2647	123.76	112.48	−188.596 869	0.02

[a]Frozen core calculation.
[b]Energy of the symmetry broken solution minus the symmetry constrained solution at the C_{2v} optimized geometry.

RESULTS AND DISCUSSION

UHF and single reference determinant calculations

The structures and energies of symmetry constrained UHF calculations on the $^2B_2$ and $^2A_1$ states of σ-HCO_2 are collected in Tables I and II, along with the results of correlated methods based on these UHF reference determinants. The results obtained with the hybrid density functional method B3LYP are also given. In the $^2B_2$ state, an a_1 orbital is doubly occupied and a b_2 orbital is singly occupied; in the $^2A_1$ state, the occupancy is reversed. Sketches of these orbitals are shown in Scheme 3. The $^2B_2$ state is lower in energy and has a smaller OCO angle than the $^2A_1$ state because the a_1 orbital is O–O bonding. The a_1 orbital also has C–H bonding character; since this orbital singly occupied in $^2A_1$ state, the C–H bond is significantly longer bond than in the $^2B_2$ state. Subsequent improvements of the wavefunctions do not change these qualitative differences between the $^2B_2$ and $^2A_1$ state

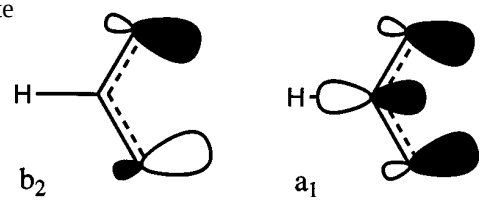

Scheme 3. b_2 and a_1 orbitals for HCO_2.

At the C_{2v} geometry, the symmetry broken UHF/6-31G* solutions are 9.8 and 6.3 kcal/mol lower than the $^2B_2$ and $^2A_1$ symmetry constrained UHF calculations, respectively (Tables I and II). With UMPn methods, the symmetry broken states are much higher than the symmetry constrained calculations, indicating that perturbative treatment of electron correlation can give rather misleading energetics for spatial symmetry breaking, similar to UMPn calculations on spin contaminated systems[50] (i.e., spin symmetry broken wave functions). The energy difference between the symmetry broken and constrained wavefunctions is significantly less for UQCISD calculations, much less for UCCSD and essentially zero for UBD. Perturbative corrections for the triples makes the energy difference significantly worse for UQCISD, but have little or no effect on the CC or BD calculations. This parallels the problems in QCISD(T) calculations for other cases with large T_1 amplitudes.[52–54]

Geometry optimization of the symmetry broken solutions results in structures with unequal C–O bond lengths that are 1–13 kcal/mol lower in energy than the symmetric structures (Table III). The changes are largest at the UHF level, with C–O bond lengths that differ by 0.15 Å. The UMP2 calculations reduce this difference slightly. The difference in the C–O bond lengths is much smaller at the UQCISD level, but perturbative triples make matters worse. From the very small energy difference between the symmetry constrained and symmetry broken calculations at the BD level in Tables I and II, one would expect the symmetry broken BD calculations to yield a structure with nearly equal C–O bond lengths. The energy is lower than either the $^2B_2$ or $^2A_1$ solution and the difference in the bond lengths in the BD calculation is nearly as large as at the UHF level. Thus the BD calculations do not solve the symmetry breaking problem.

2×2 Nonorthogonal CI calculations

Tables IV and V present the results of the 2×2 nonorthogonal CI calculations. The potential energy surfaces are stabilized by about 18 kcal/mol compared to the UHF calculations and the $^2B_2$ state is lower in energy than the $^2A_1$ state. There is a noticeable change in geometry for the minima, especially for the $^2A_1$ state.

TABLE II. Energies and optimized geometries of $^2A_1$ σ-HCO_2 calculated with single reference, symmetry constrained wave functions and the 6-31G* basis set.

Method	CH (Å)	CO (Å)	HCO (degree)	OCO (degree)	Energy (Hartree)	ΔE^b (kcal/mol)
HF	1.1978	1.1943	106.24	147.52	−188.081 961	−6.27
B3LYP	1.1551	1.2310	108.11	143.78	−189.077 678	0.00
MP2	1.1697	1.2328	106.85	146.30	−188.583 088	18.32
QCISD	1.1585	1.2339	107.95	144.10	−188.587 194	−4.55
QCISD(T)[a]	1.1558	1.2421	108.25	143.50	−188.596 328	6.99
CCSD	1.1606	1.2299	107.81	144.38	−188.582 928	0.14
CCSD(T)	1.1586	1.2380	108.05	143.90	−188.604 086	1.49
BD[a]	1.1630	1.2287	107.73	144.54	−188.570 267	0.02

[a]Frozen core calculation.
[b]Energy of the symmetry broken solution minus the symmetry constrained solution at the C_{2v} optimized geometry.

TABLE III. Energies and optimized geometries of $^2A'$ σ-HCO_2 calculated with single reference, symmetry broken wave functions and the 6-31G* basis set.

Method	CH (Å)	CO (Å)	CO′ (Å)	HCO′ (degree)	OCO′ (degree)	Energy (Hartree)	ΔE^b (kcal/mol)
HF	1.0890	1.3240	1.1770	126.20	124.60	−188.130 115	−12.78
MP2	1.1064	1.3025	1.1908	125.97	125.50	−188.571 305	−6.54
QCISD	1.0987	1.2817	1.2478	123.94	116.06	−188.598 024	−0.68
QCISD(T)[a]	1.1012	1.3314	1.2228	115.93	116.31	−188.595 272	−10.90
BD[a]	1.1083	1.3369	1.2048	126.27	125.49	−188.579 691	−3.07

[a]Frozen core calculation.
[b]Energy of the symmetry broken solution at the $^2A'$ optimized geometry minus the symmetry broken solution at the $^2B_2$ optimized geometry given in Table I.

TABLE IV. Energies and optimized geometries of $^2B_2$ σ-HCO_2 calculated with multireference wave functions.

Method	CH (Å)	CO (Å)	HCO (degree)	OCO (degree)	Energy (Hartree)
2×2 CI[a]	1.0828	1.2399	121.88	116.24	−188.131 144
2×2 CI(approx MP2)[a,b]	1.0956	1.2645	123.85	112.30	−188.580 546
2×2 CI(MP2)[a,c]	1.0943	1.2629	124.57	110.86	−188.582 284
MCSCF[d]	1.098	1.268	123.9	112.2	−188.328 968
MCSCF[e]	1.084	1.264	123.7	112.5	−188.345 42
MRCI[d]	1.099	1.268	123.7	112.6	−188.402 308
CASPT2[e]	1.092	1.263	123.5	113.0	−188.726 99
EOM-CC[f]	1.100	1.258	123.6	112.8	−188.688 88

[a]Using the 6-31G* basis set.
[b]Approximate MP2 corrected 2×2 CI using Eq. (9).
[c]MP2 corrected 2×2 CI using Eq. (5).
[d]From Ref. 17 using a Dunning DZP basis set.
[e]From Ref. 18 using an ANO basis set.
[f]From Ref. 22 using a Dunning DZP basis set.

TABLE V. Energies and optimized geometries of $^2A_1$ σ-HCO_2 calculated with multireference wave functions.

Method	CH (Å)	CO (Å)	HCO (degree)	OCO (degree)	Energy (Hartree)
2×2 CI[a]	1.1105	1.2238	110.51	138.98	−188.118 165
2×2 CI(approx MP2)[a,b,d]	1.1543	1.2348	108.35	143.30	−188.569 962
2×2 CI(MP2)[a,c,d]	1.1519	1.2319	108.35	143.30	−188.572 399
CASPT2[e]	1.154	1.236	107.75	144.5	−188.729 33
EOM-CC[f]	1.149	1.233	108.1	143.9	−188.682 387

[a]Using the 6-31G* basis set.
[b]approximate MP2 corrected 2×2 CI using Eq. (9).
[c]MP2 corrected 2×2 CI using Eq. (5).
[d]Valley–ridge inflection point.
[e]From Ref. 18 using an ANO basis set.
[f]From Ref. 22 using a Dunning DZP basis set.

Figure 1 shows a series of potential energy curves as a function of the OCO angle. The $^2B_2$ state is lower in energy at small bond angles, while the $^2A_1$ state is more stable at larger angles. By varying the OCO angle, the effects of symmetry breaking can be studied without the lowering in symmetry that accompanies asymmetric C–O bond stretching. As expected, the symmetry broken UHF curve is lower in energy than both symmetry constrained solutions and has only one minimum at an intermediate angle. The 2×2 nonorthogonal CI calculations yield two potential energy curves of the correct symmetry and energy ordering. Surprisingly, the crossing between the $^2B_2$ and $^2A_1$ curves occurs at nearly the same angle at both the symmetry constrained UHF and 2×2 nonorthogonal CI levels of theory.

Unlike the symmetry constrained UHF calculations, the 2×2 CI calculations are continuous over asymmetric large displacements. In the MR-CI calculations of Peyerimhoff and coworkers[20] the energy decreases as one CO bond is lengthened and the other shortened. At the 2×2 CI level, the $^2B_2$ state is stable with respect to asymmetric CO stretch. However, a frequency calculation shows that the $^2B_2$ stationary point is a first order saddle point at the 2×2 nonorthogonal CI level of theory. The transition vector contains a large HCO bend component and should be perhaps best described

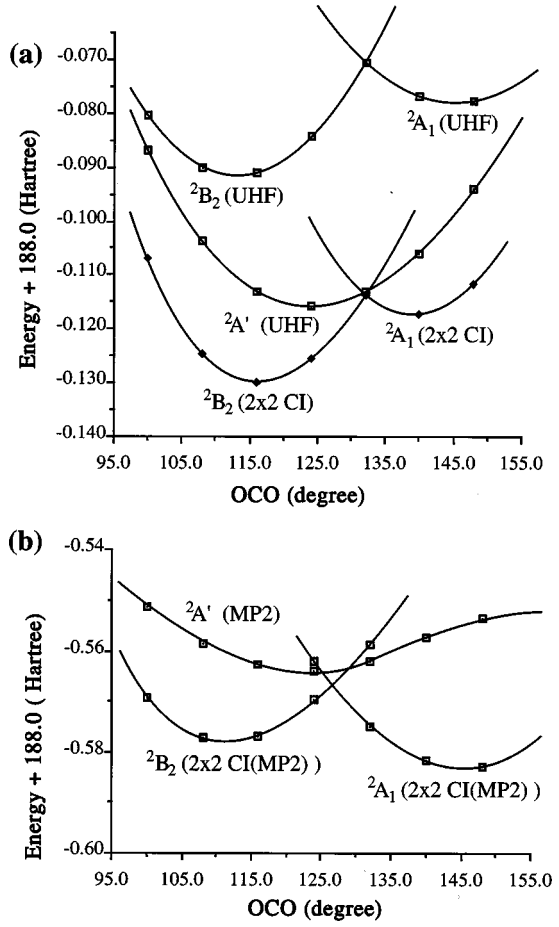

FIG. 1. Energy curves for the $^2B_2$, $^2A_1$, and $^2A'$ states of σ-HCO_2 as a function of the OCO angle. (a) UHF and 2×2 nonorthogonal CI, (b) UMP2 and 2×2 nonorthogonal CI with MP2 corrections [Eq. (5)].

as an asymmetric deformation rather than an asymmetric CO stretch.

Similar to Feller's MCSCF study[19] and Stanton's EOM-CC calculations with medium size basis sets,[22] the 2×2 nonorthogonal CI level produce an $^2A_1$ structure is a first order saddle point (one imaginary frequency, $2151i$ cm^{-1}). The two mirror image $^2A'$ minima are found 0.38 kcal/mol below the $^2B_2$ transition state with geometries closely resembling the Hartree–Fock structure. Very large basis set calculations with the EOM-CC method[22] suggest that the $^2A_1$ structure may be a shallow minimum on a very flat potential energy surface. At the UHF level of theory, the $^2A_1$ portion of the potential energy surface shows a very small barrier for CH dissociation (0.12 kcal/mol). In the CASSCF calculations by Rauk *et al.*[18] the $^2A_1$ structure dissociates to $H+CO_2$ without a barrier. Attempts to locate the $^2A_1$ transition state for H loss at the 2×2 CI level were unsuccessful, since the instability of the UHF solution disappeared before a saddle point for dissociation could be reached. One can argue that the 2×2 CI procedure may be unsuited for this portion of the potential energy surface since inclusion of the C–H bond breaking configuration becomes more and more important and it should at least be treated by a 4×4 CI, for example.

MP2 corrections to the 2×2 nonorthogonal CI calculations

Tables IV and V list the optimized geometries for the $^2B_2$ and $^2A_1$ structures using the MP2 corrected 2×2 CI. Both procedures outlined in Eq. (5) and in Eq. (9) are in good agreement with the CASPT2 results of Rauk *et al.*,[18] the MRCI results of McLean *et al.*[17] and the EOM-CC calculations of Stanton.[22] The geometries obtained with the correlated methods based on single reference determinants (Tables I and II) are also in good agreement with these calculations. Vibrational frequencies in Tables VI show that the $^2B_2$ configuration is a minimum at both MP2 corrected 2×2 CI levels, confirming that the C_{2v} symmetry structure is a minimum. The vibrational frequencies are in good agreement with the MRCI, CASPT2 and EOM-CC values. The largest difference is for the asymmetric deformation mode. The calculations listed in Tables VI, along with larger basis set EOM-CC calculations[22] indicate the frequency for this mode should be between 1000 and 1300 cm^{-1}.

The CASPT2 and EOM-CC calculations of the $^2A_1$ structure are minima with respect to C–H dissociation. However, a stationary point could not be located on the $^2A_1$ potential energy with the MP2 corrected 2×2 CI calculations. At larger CH distances and OCO angles, there is a single

TABLE VI. Vibrational frequencies of $^2B_2$ σ-HCO_2 calculated with various theories.

Method	b_2 asym. def.	a_1 sym. bend	b_1 oop bend	b_2 asym bend	a_1 sym. str.	a_1 CH stretch
2×2 CI[a]	703*i*	790	1165	1426	1594	3328
2×2 CI(approx MP2)[a,b]	986	629	989	1228	1486	3259
2×2 CI(MP2)[a,c]	1215	701	1030	1332	1516	3186
MCSCF[d]	649	594	*n/a*	1313	1479	3184
MRCI[d]	961	646	*n/a*	1314	1477	3197
CASPT2[e]	1287	624	1008	1287	1437	3053
EOM-CC[f]	1010	650	1027	1318	1513	3170
B3LYP[a]	1125	646	1029	1306	1509	3080

[a]Using the 6-31G* basis set.
[b]Approximate MP2 corrected 2×2 CI using Eq. (9).
[c]MP2 corrected 2×2 CI using Eq. (5).
[d]From Ref. 17 using a Dunning DZP basis set.
[e]From Ref. 18 using an ANO DZP basis set.
[f]From Ref. 22 using a Dunning DZP basis set.

minimum with respect to asymmetric deformation. At short CH distances and small OCO angles, the $^2A_1$ state is a maximum with respect to asymmetric deformation and there are two valleys either side of the ridge. Between these extremes there is a branching point or valley–ridge inflection point. The approximate location of this point (Table V) was obtained by performing constrained optimizations at various OCO angles and testing the stability in the space of the two CO bond lengths and the HCO angle. Surprisingly, the branching structure is very similar to the stationary point found by other methods. This apparent coincidence deserves further study.

CONCLUSIONS

This study shows that a 2×2 nonorthogonal CI along with MP2 corrections can successfully treat systems that have spatial symmetry breaking of the SCF wave function. The most important features of the $^2B_2$-HCO_2 potential energy surface are properly described by this procedure. Compared to the large MCSCF, MRCI, CASPT2, or EOM-CC calculations typically needed for these systems, the 2×2 nonorthogonal CI with perturbative corrections for dynamic correlation requires little computational effort, similar to one or two MP4SDQ calculations or CCSD iterations. The cost of the simpler model is comparable to two MP2 calculations. This procedure may be useful in the studies of chemical systems with symmetry breaking problems or Jahn–Teller interactions.

ACKNOWLEDGMENT

This work was supported by a Grant from the National Science Foundation (CHE 94-00678).

APPENDIX

The matrix elements between nonorthogonal determinants can be evaluated by expanding the orbitals for one determinant in terms of the orbitals for the other determinant. The spin orbitals for both wavefunctions can be written in terms of basis functions χ_μ

$$\phi_i=\sum c_{\mu i}\chi_\mu;\quad \langle\phi_i|\phi_j\rangle=\delta_{ij};$$
$$\phi_i'=\sum c'_{\mu i}\chi_\mu;\quad \langle\phi_i'|\phi_j'\rangle=\delta_{ij}. \tag{A1}$$

The spin orbitals of one wave function can then be expressed in terms of the spin orbitals of the other wave function and the overlap between the orbitals

$$\phi_i'=\sum S_{ip}\phi_p=\sum s_{ij}\phi_j+\sum \tilde{s}_{ia}\phi_a;$$
$$S_{pq}=\langle\phi_p'|\phi_q\rangle=\sum c'_{\mu p}c_{\nu q}\langle\chi_\mu|\chi_\nu\rangle, \tag{A2}$$

where indices i, j, etc., run over occupied orbitals, a, b, etc., run over unoccupied orbitals and p, q, etc., run over all orbitals. For convenience, the overlap between ϕ and ϕ' is split into the occupied–occupied block, s, and the occupied–virtual block, $\tilde{s}$. The wave function Ψ_0' can be expanded in terms of Ψ_0 and single, double and higher excitations of Ψ_0

$$\Psi_0'=\left|\left(\sum S_{1p}\phi_p\right)\left(\sum S_{2q}\phi_q\right)\cdots\left(\sum S_{nr}\phi_r\right)\right|$$
$$=a_0\Psi_0+\sum a_i^a\Psi_i^a+\sum a_{ij}^{ab}\Psi_{ij}^{ab}+\cdots. \tag{A3}$$

The matrix elements between two nonorthogonal configurations is given by[55]

$$\langle\Psi_0|\mathbf{H}|\Psi_0'\rangle=\sum\langle\phi_i|\mathbf{h}|\phi_j\rangle C(i|j)+\sum\langle\phi_i\phi_j|\phi_k\phi_l\rangle C(ij|kl),$$
$$\langle\Psi_0|\Psi_0'\rangle=\mathrm{Det}(s), \tag{A4}$$

where $C(i|j)$ is the cofactor arising from s by deleting row i and column j, and $C(ij|kl)$ from deleting rows i and j, and columns k and l. $C(i|j)$ is given by

$$C(i|j)=(s^{-1})_{ij}\mathrm{Det}(s)=(s^{-1})_{ij}\langle\Psi_0|\Psi_0'\rangle. \tag{A5}$$

By further application of Kramer rule for matrix inversion or by use of the Jacobi ratio theorem[56] $C(ij|kl)$ can be expressed as

$$C(ij|kl)=[C(i|k)C(j|l)-C(i|l)C(j|k)]/\mathrm{Det}(s)$$
$$=((s^{-1})_{ik}(s^{-1})_{jl}-(s^{-1})_{il}(s^{-1})_{jk})\langle\Psi_0|\Psi_0'\rangle. \tag{A6}$$

Alternatively, the necessary matrix elements can be evaluated readily if the amplitudes are known

$$\langle\Psi_0|\mathbf{H}|\Psi_0'\rangle=a_0\langle\Psi_0|\mathbf{H}|\Psi_0\rangle+\sum a_{ij}^{ab}\langle\Psi_0|\mathbf{H}|\Psi_{ij}^{ab}\rangle. \tag{A7}$$

After rearrangement of the expressions for the cofactors, the amplitudes can be written as:

$$a_0=\mathrm{Det}(s),$$
$$a_i^a=\sum C(k|i)\tilde{s}_{ka}=\sum (s^{-1})_{ki}\tilde{s}_{ka}a_0,$$
$$a_{ij}^{ab}=(a_i^a a_j^b-a_j^a a_i^b)/a_0. \tag{A8}$$

This result can be shown more directly by considering the overlap between Ψ_0' and each excited determinant of interest. Figari and Magnesco[57] and VerBeek and VanLenthe[58,59] have given more general expressions for matrix elements between nonorthogonal configurations. Once the expansion coefficients are known, the off-diagonal CI matrix elements can be constructed in a way similar to the MP2 procedure.

[1] G. W. Flynn, Science **246**, 1009 (1988).
[2] K. Kudla and G. C. Schatz, J. Phys. Chem. **95**, 8267 (1991).
[3] G. C. Schatz, Rev. Mod. Phys. **61**, 669 (1989).
[4] G. C. Schatz, M. S. Fitzcharles, and L. B. Harding, Faraday Discuss. Chem. Soc. **84**, 359 (1987).
[5] C. Wittig, S. Sharpe, and R. A. Beaudet, Acc. Chem. Res. **21**, 341 (1988).
[6] K. Saito, T. Kakumoto, H. Kuroda, S. Torii, and A. Imamura, J. Chem. Phys. **80**, 4989 (1984).

[7] J. D. Goddard, Y. Yamaguchi, and H. F. Schaefer, J. Chem. Phys. **96**, 1158 (1991).
[8] J. S. Francisco, J. Chem. Phys. **96**, 1167 (1991).
[9] J. Paldus and A. Veillard, Mol. Phys. **35**, 445 (1978).
[10] A. F. Voter and W. A. Goddard, Chem. Phys. **57**, 253 (1981).
[11] E. R. Davidson and W. T. Borden, J. Phys. Chem. **87**, 4783 (1983).
[12] C. F. Jackels and E. R. Davidson, J. Chem. Phys. **65**, 2941 (1976).
[13] C. F. Jackels and E. R. Davidson, J. Chem. Phys. **64**, 2908 (1976).
[14] C. P. Blahous, B. F. Yates, Y. Xie, and H. F. Schaefer, J. Chem. Phys. **93**, 8105 (1990).
[15] J. Gauss, J. F. Stanton, and R. J. Bartlett, J. Chem. Phys. **95**, 2639 (1991).
[16] N. Burton, Y. Yamaguchi, I. L. Alberts, and H. F. Schaefer, J. Chem. Phys. **95**, 7466 (1991).
[17] A. D. McLean, B. H. Lengsfield, J. Pacansky, and Y. Ellinger, J. Chem. Phys. **83**, 3567 (1985).
[18] A. Rauk, D. Yu, P. Borowski, and B. Roos, Chem. Phys. **197**, 73 (1995).
[19] D. Feller, E. S. Huyser, W. T. Borden, and E. R. Davidson, J. Am. Chem. Soc. **105**, 1459 (1983).
[20] S. D. Peyerimhoff, P. S. Skell, D. D. May, and R. J. Buenker, J. Am. Chem. Soc. **104**, 4515 (1982).
[21] J. F. Stanton and J. Gauss, J. Chem. Phys. **101**, 8938 (1994).
[22] J. F. Stanton and N. S. Kadagathur, J. Mol. Struct. **376**, 469 (1996).
[23] J. Paldus and J. Cizek, Chem. Phys. Lett. **3**, 1 (1969).
[24] J. Paldus and J. Cizek, J. Chem. Phys. **52**, 2919 (1970).
[25] J. Paldus and M. Benard, J. Chem. Phys. **72**, 6546 (1980).
[26] A. F. Voter and W. A. Goddard, J. Am. Chem. Soc. **108**, 2830 (1986).
[27] R. L. Martin, J. Chem. Phys. **74**, 1852 (1981).
[28] R. Murphy, H. F. Schaefer, R. H. Nobes, L. Radom, and R. S. Pitzer, Int. Rev. Phys. Chem. **5**, 229 (1986).
[29] J. Paldus and J. Cizek, J. Chem. Phys. **47**, 3976 (1967).
[30] J. Paldus, J. Cizek, and B. A. Keating, Phys. Rev. A **8**, 640 (1973).
[31] J. Paldus and E. Chin, Int. J. Quantum Chem. **24**, 373, 395 (1983), and references therein.
[32] C. Liang and H. F. Schaefer, Chem. Phys. Lett. **169**, 150 (1990).
[33] P. O. Löwdin, Adv. Chem. Phys. **14**, 283 (1969), and references therein.
[34] H. Fukutome, Int. J. Quantum Chem. **20**, 955 (1981), and references therein.
[35] J. F. Stanton, J. Gauss, and R. J. Bartlett, J. Chem. Phys. **94**, 4084 (1991).
[36] W. D. Allen, D. A. Horner, R. B. Remington, and H. F. Schaefer, Chem. Phys. **133**, 11 (1989).
[37] L. Englebrecht and B. Liu, J. Chem. Phys. **78**, 3097 (1983).
[38] J. D. Watts, J. F. Stanton, J. Gauss, and R. J. Bartlett, J. Chem. Phys. **94**, 4320 (1991).
[39] J. D. Watts and R. J. Bartlett, J. Chem. Phys. **95**, 6652 (1991).
[40] O. Goscinski, Int. J. Quantum Chem., Quantum Chem. Symp. **19**, 51 (1986).
[41] A. P. L. Rendell, G. B. Bacskay, and N. S. Hush, J. Am. Chem. Soc. **110**, 8343 (1988).
[42] J. B. Bacskay, G. Bryant, and N. S. Hush, Int. J. Quantum Chem. **31**, 471 (1987).
[43] H. Agren, P. Bagus, and B. O. Roos, Chem. Phys. Lett. **82**, 505 (1981).
[44] L. S. Cederbaum and W. Domcke, J. Chem. Phys. **66**, 5084 (1977).
[45] R. L. Martin and E. R. Davidson, Phys. Rev. A **16**, 1341 (1977).
[46] P. S. Bagus and H. F. Schaefer, J. Chem. Phys. **56**, 224 (1972).
[47] B. J. Roos, K. Andersson, M. F. Fülscher, P.-A. Malmqvist, L. Serrano-Andrés, K. Pierloot, and M. Merchán, Adv. Chem. Phys. **93**, 219 (1996).
[48] P. C. Hiberty, S. Humbel, and P. Archirel, J. Phys. Chem. **98**, 11697 (1994).
[49] D. L. Cooper, J. Gerratt, and M. Raimondi, Adv. Chem. Phys. **69**, 319 (1987), and references therein.
[50] H. B. Schlegel, J. Chem. Phys. **84**, 4530 (1986).
[51] M. J. Frisch, G. W. Trucks, H. B. Schlegel, P. M. W. Gill, B. G. Johnson, M. A. Robb, J. R. Cheeseman, T. Keith, G. A. Petersson, J. A. Montgomery, K. Raghavachari, M. A. Al-Laham, V. G. Zakrzewski, J. V. Ortiz, J. B. Foresman, J. Cioslowski, B. B. Stefanov, A. Nanayakkara, M. Challacombe, C. Y. Peng, P. Y. Ayala, W. Chen, M. W. Wong, J. L. Andres, E. S. Replogle, R. Gomperts, R. L. Martin, D. J. Fox, J. S. Binkley, D. J. Defrees, J. Baker, J. P. Stewart, M. Head-Gordon, C. Gonzalez, and J. A. Pople, GAUSSIAN 94 (Gaussian, Inc., Pittsburgh, PA, 1995).
[52] J. Hrusak, S. Ten-no, and S. Iwata, J. Chem. Phys. **106**, 7185 (1997).
[53] J. D. Watts, M. Urban, and R. J. Bartlett, Theor. Chim. Acta **90**, 341 (1995).
[54] M. Böhme and G. Frenking, Chem. Phys. Lett. **224**, 195 (1994).
[55] P. O. Löwdin, Phys. Rev. **97**, 1474 (1955).
[56] A. C. Aitken, *Determinants and Matrices* (Oliver and Boyd, 1958), pp. 97.
[57] G. Figari and V. Magnasco, Mol. Phys. **55**, 319 (1985).
[58] J. Verbeek and J. Van Lenthe, Int. J. Quantum Chem. **40**, 201 (1991).
[59] J. Verbeek and J. Van Lenthe, J. Mol. Struct.: THEOCHEM **75**, 115 (1991).